

The mass of the neutron star in SMC X-1

A.K.F. Val Baker, A.J. Norton, and H. Quaintrell

Department of Physics and Astronomy, The Open University, Walton Hall, Milton Keynes MK7 6AA, U.K.

Accepted 01/07/2005 Received 16/03/2005

Abstract. We present new optical spectroscopy of the eclipsing binary pulsar Sk 160/SMC X-1. From the He I absorption lines, taking heating corrections into account, we determine the radial velocity semi-amplitude of Sk 160 to be $21.8 \pm 1.8 \text{ km s}^{-1}$. Assuming Sk 160 fills its Roche-lobe, the inclination angle of the system is $i = 65.3^\circ \pm 1.3^\circ$ and in this case we obtain upper limits for the mass of the neutron star as $M_x = 1.21 \pm 0.10 M_\odot$ and for Sk 160 as $M_o = 16.6 \pm 0.4 M_\odot$. However if we assume that the inclination angle is $i = 90^\circ$, then the ratio of the radius of Sk 160 to the radius of its Roche-lobe is $\beta = 0.79 \pm 0.02$, and the lower limits for the masses of the two stars are $M_x = 0.91 \pm 0.08 M_\odot$ and $M_o = 12.5 \pm 0.1 M_\odot$. We also show that the He II 4686Å emission line tracks the motion of the neutron star, but with a radial velocity amplitude somewhat less than that of the neutron star itself. We suggest that this emission may arise from a hotspot where material accreting via Roche lobe overflow impacts the outer edge of an accretion disc.

Key words. binaries: close – stars: neutron – stars: individual: SMC X-1 – stars: individual: Sk 160 – stars: fundamental parameters

1. Introduction

Eclipsing X-ray pulsars offer a means of directly measuring neutron star masses. However, only 7 such systems are currently known and the neutron star masses in each case are not determined to high accuracy. If the situation can be improved, the equation of state for nuclear matter may be constrained, so testing theories that describe it. To this end that we have carried out the present study of SMC X-1. The determination of the system masses follows from measuring the semi-amplitude of the neutron star's radial velocity (RV) curve (K_x , from X-ray pulse timing delays), the X-ray eclipse half angle (θ_e), and the semi-amplitude of the companion star's RV curve (K_o , from absorption line optical spectroscopy); for details see e.g. Ash et al. (1999) and Quaintrell et al. (2003). It is important to note that the relevant equations can only be solved by assuming a value for either the system inclination angle (i) or the ratio of the radius of the optical companion star to that of its Roche lobe (β), see Equation (4) of Quaintrell et al. (2003). Previous studies of SMC X-1 have generally assumed the companion star is Roche lobe-filling (i.e. $\beta = 1$) and so obtained masses that are only relevant in this limit; we return to this later.

The optical counterpart to SMC X-1 is the B0 I supergiant, Sk 160 (Webster et al. 1972; Liller 1972). The X-ray source has a pulse period of 0.72 s and exhibits an eclipse duration of $0.610 \pm 0.019 \text{ d}$ (Primini et al. 1976)

in the 3.892 d orbit, corresponding to $\theta_e = 28.2^\circ \pm 0.9^\circ$. Timing studies of the X-ray pulsations (Levine et al. 1993) give $(a_x \sin i) = 53.4876 \pm 0.0004 \text{ lt sec}$ for the projected semi-major axis and indicate a circular orbit with $e < 0.00004$. The corresponding RV amplitude is $K_x = 299.607 \pm 0.002 \text{ km s}^{-1}$. The X-ray emission from SMC X-1 has also been found to exhibit a long quasi-stable super-orbital period of 50–60 days, believed to be a result of obscuration of the neutron star by a precessing accretion disk (e.g. Wojdowski et al. 1998). The mass transfer in SMC X-1 probably has significant contributions from Roche-lobe overflow (Khruzina & Cherepashchuk 1983; van Paradijs & Kuiper 1984), as the stellar winds observed in Sk 160 are not strong enough to power the accretion (Hammerschlag-Hensberge, Kallman & Howarth 1984).

Previous attempts to derive the orbital parameters of SMC X-1 have been made by Primini et al. (1976), Hutchings et al. (1977), Reynolds et al. (1993) and van der Meer et al. (2005). Reynolds et al. (1993) were the first to account for heating of the donor star by the X-ray flux from the neutron star. This heating has the effect of significantly altering the observed RV amplitude and so distorting the inferred neutron star mass. However van Kerkwijk et al. (1995) pointed out the uncertainties introduced in this approach by not allowing for the presence of an accretion disk, whose shadow on the face of the giant star may reduce the effect of X-ray heating. The most recent analysis by van der Meer et al. (2005), like several earlier investigations, found a low value for the neutron star

mass, $M_x = 1.05 \pm 0.09 M_\odot$, but they too did not account for any heating correction in their analysis. It should also be noted that each of the previous mass determinations implicitly assumed the companion star to fill its Roche lobe in order to solve for the system parameters, so the masses are in effect upper limits in each case.

2. Observations

Our observations were obtained from 30th August – 18th September 2000 using the 1.9 metre Radcliff telescope at the Sutherland Observatory. The grating spectrograph was used with a reciprocal dispersion of $0.5 \text{ \AA}/\text{pixel}$, spanning the wavelength range $4300 - 5100 \text{ \AA}$. Over the course of 3 weeks (1 week on, 1 week off, 1 week on) we obtained 56 usable spectra of Sk 160 on 9 nights, mostly during the first week of observations (see Table 2). We note that these observations just preceded the coordinated HST/Chandra campaign on SMC X-1 reported by Vrtilik et al. (2001), and occurred during a low state of the ~ 55 d super-orbital cycle, as indicated by the *RXTE* ASM lightcurve.

We also observed the RV standard star HD6655, an F8 V star with an accurately known radial velocity of $+15.5 \text{ km s}^{-1}$, on each night. In addition, on the last night, we observed a template star of similar spectral type to Sk 160, for cross-correlation with our target spectra. This was HR1174, a B3 V star, which was also used as the cross-correlation template by Reynolds et al. (1993).

3. Data Reduction

All spectra were reduced using standard IRAF¹ routines; Figure 1 shows a median, continuum normalised spectrum of Sk 160. Note that the apparent double peak in the He II 4686Å emission line is the result of sampling this line mostly at the quadrature phases of the system. The median spectrum therefore shows two peaks separated by $\approx 8\text{Å}$ corresponding to a $\approx 500 \text{ km s}^{-1}$ velocity difference. In order to check the stability of the observations from night to night, we cross-correlated the individual spectra of the RV standard star HD6655 against a single spectrum of this object from the middle of the run. These were all consistent with zero shift from night to night.

Having confirmed the stability of the system, each individual spectrum of Sk 160 was cross-correlated against the median spectrum of the template star, HR1174. Only regions between 4370–4500Å, 4700–4735Å and 4900–5060Å were used, spanning several He I absorption lines. These regions were selected to exclude the Balmer lines which were found to show large, random changes from one spectrum to the next, and no clear trend in their RVs. It is well known that Balmer lines in high mass stars may be contaminated by emission from the star’s wind and so may

¹ IRAF is distributed by the National Optical Astronomy Observatory, which is operated by the Association of Universities for Research in Astronomy, Inc., under cooperative agreement with the National Science Foundation.

not accurately reflect the orbital RV in a binary system. The extent of the emission contamination depends on the strength of the stellar wind and is reduced for higher level Balmer transitions. Final heliocentric RVs corresponding to each spectrum of Sk 160 were calculated from the cross-correlation results by applying the heliocentric velocity corrections and then offsetting the result by the RV of HR1174, measured by fitting Gaussians to the He I lines in its spectrum as $+16.7 \text{ km s}^{-1}$. These final RVs are listed in Table 2 along with their 1σ uncertainties, and plotted in Figure 2.

Orbital phases corresponding to each spectrum were calculated using the ephemeris from Wodjowski et al. (1998), which gives the centre time of the N th eclipse as $t_N/\text{MJED} = 42836.18278(20) + 3.89229090(43)N - (6.953(28) \times 10^{-8})N^2$. Numbers in brackets indicate the uncertainties in the last decimal places in each case. The orbital period at the time of our observations, ~ 2300 periods after the reference time of this ephemeris, is $P = 3.891971(1)\text{d}$. Also included in Figure 2 are the RV measurements of Reynolds et al. (1993), with phases calculated according to the revised ephemeris above.

4. Data analysis

4.1. System parameters from the raw He I RV curve

The data shown in Figure 2 were fitted with a sinusoid, allowing the mean level and amplitude as free parameters. The semi-amplitude of the RV curve is $K_o = 18.0 \pm 1.8 \text{ km s}^{-1}$ and the systemic velocity is $\gamma = 174.1 \pm 1.5 \text{ km s}^{-1}$; these values are listed in Table 1.

The masses of the stars were calculated following the procedure of Ash et al. (1999) and Quaintrell et al. (2003), using the Monte Carlo method for uncertainty determination described therein. As SMC X-1 has a circular orbit, the Roche lobe filling factor ($\beta = R_o/R_L$) will not vary, but in the absence of an exact value for the radius of the companion star’s Roche lobe we cannot determine β uniquely. Since mass transfer in SMC X-1 has significant contributions from Roche lobe overflow, but Sk 160 is unlikely to be overfilling its Roche lobe, we can however set an upper limit of $\beta \leq 1.0$, which in turn sets a lower limit on i . Conversely if we set an upper limit on the inclination angle of $i = 90^\circ$, we obtain a lower limit for β . Given these two extremes, upper and lower limits on the mass of both the neutron star and the optical companion may be calculated, as shown in the two left hand columns of Table 1. Solutions lying between the two extremes, corresponding to intermediate values of i and β , are of course also valid.

4.2. X-ray heating corrections

RV measurements of the optical companion in a binary system reflect its motion about the centre of light. In systems with Keplerian orbits, the centre of light should be roughly coincident with the centre of mass. However, X-ray heating of the optical companion can lead to an offset

Table 1. System parameters for Sk 160/SMC X-1. The two values for K_o are those resulting from fitting the HeI absorption line RV curve without and with heating corrections respectively. The 4 columns for the inferred parameters are the limiting values assuming $\beta = 1$ and $i = 90^\circ$ for each of the values of K_o as discussed in the text.

Parameter	Fit to raw RV curve		Fit to corrected RV curve	
$\gamma / \text{km s}^{-1}$	174.1 \pm 1.5		173.8 \pm 1.5	
$K_o / \text{km s}^{-1}$	18.0 \pm 1.8		21.8 \pm 1.8	
q	0.060 \pm 0.006		0.073 \pm 0.006	
	Roche lobe-filling (upper mass limits)	edge-on (lower mass limits)	Roche lobe-filling (upper mass limits)	edge-on (lower mass limits)
β	1.00	0.77 \pm 0.02	1.00	0.79 \pm 0.02
i / deg	64.0 \pm 1.3	90.0	65.3 \pm 1.3	90.0
M_x / M_\odot	1.01 \pm 0.10	0.73 \pm 0.08	1.21 \pm 0.10	0.91 \pm 0.08
M_o / M_\odot	16.8 \pm 0.5	12.1 \pm 0.2	16.6 \pm 0.4	12.5 \pm 0.1
a / R_\odot	27.4 \pm 0.3	24.6 \pm 0.2	27.3 \pm 0.3	24.7 \pm 0.1
R_L / R_\odot	16.7 \pm 0.3	14.9 \pm 0.1	16.3 \pm 0.2	14.8 \pm 0.1
R_o / R_\odot	16.7 \pm 0.3	11.5 \pm 0.3	16.3 \pm 0.2	11.7 \pm 0.3

between the two centres, such that the observed RVs may not represent the true motion about the centre of mass. In order to determine accurate masses from RV curves, these non-Keplerian deviations must therefore be accounted for.

To correct for the heating effects we followed Reynolds et al. (1993) and ran models using LIGHT2 (Hill 1988), a sophisticated light-curve synthesis program. In the mode used here, the program generates non-Keplerian velocity corrections by averaging a velocity based on contributions from elements of the giant star’s projected stellar disk, where each element is weighted according to the flux at that point. We note that the He I lines will be stronger on the cooler side of the star (i.e. away from the X-ray source) and this may shift the light centre in the opposite direction to the flux weighting correction which LIGHT2 applies. The net effect of the true heating correction may therefore be smaller than calculated here.

Due to the limitations of LIGHT2 we were unable to accurately represent the dimensions of the neutron star in the model. Instead, we set the radius and polar temperature of the object representing the neutron star to produce a blackbody luminosity equivalent to the observed X-ray luminosity, which is essentially all that matters to calculate the heating correction. We used $L_x = 2.4 \times 10^{38} \text{ erg s}^{-1}$ (Paul et al. 2002), which agrees well with the value of $L_x = 2.0 \times 10^{38} \text{ erg s}^{-1}$ that we determined using the *RXTE* ASM flux for the epoch of observation, assuming a simplified X-ray spectral shape and a distance to the SMC of $D = 60.6 \text{ kpc}$ (Hilditch et al. 2005).

The initial values for i and q input to LIGHT2 were those obtained from the Monte Carlo analysis using the raw value for Sk 160’s RV amplitude. Having calculated the RV correction at the phase corresponding to each of the spectra, the individual RV measurements were adjusted accordingly, and a new solution for the RV amplitude was found. This amplitude was fed into the Monte Carlo program to determine new values for i and q , and these values were then fed back into LIGHT2 to recalculate the RV corrections. We found that the code was required to run through 3 iterations before there was no further

change in the heating corrections. The results of this process are shown in the two right hand columns of Table 1 and the final corrected RV curve is shown in Figure 3, with the data listed in Table 2.

4.3. He II 4686Å emission line

Hutchings et al. (1977) noted that the He II 4686Å emission line seen from Sk 160 moves approximately in antiphase with respect to the He I lines, and follows the RV of the neutron star, albeit with a lower amplitude, i.e. $\sim 250 \text{ km s}^{-1}$ as opposed to $\sim 300 \text{ km s}^{-1}$. In order to investigate this with our data, we performed Gaussian fits to the He II emission lines in each spectrum, and plotted their heliocentric corrected velocities against phase in Figure 4; the data are listed in Table 2. In the more noisy spectra, it was not possible to measure this emission line, so there are less data points here than in Figures 2 and 3. Overplotted on these data is the best-fit sinusoid which has an amplitude of $265 \pm 8 \text{ km s}^{-1}$, a systemic velocity of $167 \pm 7 \text{ km s}^{-1}$, and a phase shift of 0.46 ± 0.01 with respect to the ephemeris of Wojdowski et al. (1998). What we see is very similar to the behaviour noted by Hutchings et al, in that the He II emission line velocity tracks the motion of the neutron star but has a lower amplitude than that of the neutron star itself. The slight phase shift from the motion of the neutron star is also similar to that seen in the He II emission line RV of Cyg X-1 (Gies & Bolton 1986a, 1986b). As noted by Hutchings et al, this might indicate an origin for the emission that lies between the neutron star and the surface of Sk 160. We suggest that a possible site for this emission may be a hot-spot where a stream of material accreting via Roche lobe overflow impacts the outer edge of the neutron star’s accretion disk.

5. Discussion

Our final value for γ of $173.8 \pm 1.5 \text{ km s}^{-1}$ is in excellent agreement with the value obtained by Reynolds et al. (1993) from their heating corrected radial velocity curve,

namely $173.0 \pm 1.5 \text{ km s}^{-1}$. However, our raw and corrected values found for K_o and the corresponding upper limits to the neutron star mass (i.e. those corresponding to $\beta = 1$) are each lower than those found by Reynolds et al. The discrepancy could be due to the limited phase coverage of their data set and the fact that the value they assume for L_x , when determining the non-Keplerian corrections, is significantly higher than the value we used. In comparison, our raw value for K_o and the corresponding upper limit on the neutron star mass are both in good agreement with those found by van der Meer et al. (2005), namely $K_o = 20.3 \pm 0.9 \text{ km s}^{-1}$ and $M_x = 1.05 \pm 0.09 M_\odot$. In both of these previous studies, however, the authors assume that the giant star is Roche-lobe filling. Whilst this is plausible, it only gives an upper limit for the mass of the neutron star, as noted above.

There remains the question of whether an accretion disk will cast a shadow on the giant star so reducing the effect of X-ray heating, as raised by van Kerkwijk et al. (1995). In a study of Her X-1, Reynolds et al. (1997) corrected for non-Keplerian deviations using both a diskless model (LIGHT2) and a disk model. In that case the quantitative agreement between the two models was found to be good. As Her X-1 clearly has a disk, and also has a companion star that is significantly smaller than that in SMC X-1, we can assume that the absence of a disk in the LIGHT2 code has negligible effect on the heating corrections in our case.

Model calculations of Type II supernovae suggest that these events produce a bimodal distribution of initial neutron star masses, with averages within those peaks of 1.28 and 1.73 M_\odot , whereas Type Ib supernovae produce neutron stars with masses around 1.32 M_\odot (Timmes et al 1996). Neutron stars produced in Type Ia supernovae are expected to have masses close to the Chandrasekhar limit, 1.44 M_\odot (for a He white dwarf). Based on our heating-corrected mass determination of $(0.91 \pm 0.08) M_\odot - (1.21 \pm 0.10) M_\odot$ (depending on the Roche lobe filling factor), the neutron star in SMC X-1 is consistent with the first peak in the Type II supernovae bimodal neutron star mass distribution. We note that mass determinations which *do not* account for X-ray heating in SMC X-1 give a small neutron star mass that is inconsistent with *all* of the predictions above. Note also that these theoretical models do not take into account any mass that subsequently accretes in a binary system, so the theoretical values for the neutron star masses in accreting binaries are even higher.

Finally, we note the implications of our interpretation for the origin of the He II 4686Å emission line. If this arises in a stream-disk impact hot spot, it confirms that some of the accretion occurs via Roche lobe overflow, as previously surmised. It also suggests a potential test of the idea. The accretion disc in SMC X-1 is supposed to precess with a period of $\sim 55 \text{ d}$ (e.g. Wojdowski et al. 1998). In this case, the stream-disk impact site should change its location on this period, moving closer to and further away from the neutron star as the eccentric disc precesses. Both the equivalent width and the RV amplitude of the He II

emission line should therefore vary throughout the precession cycle. Unfortunately, our data do not extend over enough of the super-orbital cycle, nor are they of high enough signal-to-noise to test this, but such an investigation would be worth carrying out in future.

Acknowledgements. We are grateful to the staff of the SAAO for scheduling the observations on which this paper is based and their help during the observing run. We thank Graham Hill for the use of his LIGHT2 code and Alastair Reynolds for the radial velocities from his paper. We are indebted to Tim Harries for providing us with a linux installation of LIGHT2 and Ron Hilditch for his invaluable, patient advice helping us to get LIGHT2 to work. We also thank Sean Ryan for assistance with the intricacies of cross-correlations in iraf and an anonymous referee for several helpful suggestions to improve the paper.

References

- Ash, T.D.C., Reynolds, A.P., Roche, P., Norton, A.J., Still, M.D. & Morales-Rueda, L. 1999, MNRAS, 307, 357
 Gies, D.R. & Bolton, C.T. 1986, ApJ, 304, 371
 Gies, D.R. & Bolton, C.T. 1986, ApJ, 304, 389
 Hammerschlag-Hensberge, G., Kallman, T.R. & Howarth, I.D. 1984, ApJ, 283, 249
 Hilditch, R.W., Howarth, I.D. & Harries, T.J. 2005, MNRAS, 357, 304
 Hill, G. 1988, Light2 User Manual, Publ.Dom.Astrophys.Obs.
 Hutchings, J.B., Cowley, A.P., Osmer, P.S. & Crampton, D. 1977, ApJ, 217, 186
 Khruzina, T.S. & Cherepashchuk, A.M. 1983, Soviet Ast., 27, 35
 Levine, A., Rappaport, S., Deeter, J.E., Boynton, P.E. & Nagase, F. 1993, ApJ, 410, 328
 Liller, W. 1972, IAU Circ., No. 2469
 Paul, B., Nagase, F., Endo, T., Dotani, T., Yokogawa, J. & Nishiuchi, M. 2002, ApJ, 579, 411
 Primini, F., Clark, G.W., Lewin, W., Li, F., Mayer, W., McClintock, J., Rappaport, S. & Joss, P.C. 1976, ApJ, 210, L71
 Primini, F., Rappaport, S. & Joss, P.C. 1977, ApJ, 217, 543
 Quaintrell, H., Norton, A.J., Ash, T.D.C., Roche, P., Willems, B., Bedding, T.R., Baldry, I.K. & Fender, R.P. 2003, A&A, 401, 313
 Rappaport, S.A. & Joss, P.C. 1983, in Accretion-Driven Stellar X-ray Sources, 1-39, C.U.P.
 Reynolds, A.P., Hilditch, R.W., Bell, S.A. & Hill, G. 1993, MNRAS, 261, 337
 Reynolds, A.P., Quaintrell H., Still, M.D., Roche, P., Chakrabarty, D. & Levine, S.E. 1997, MNRAS, 288, 43
 Timmes, F.X., Woosley, S.E. & Weaver, T.A. 1996, ApJ, 457, 834
 van der Meer, A., Kaper, L., van Kerkwijk, M.H. & van den Heuvel, E.P.J. 2005, ASP Conference Series, astro-ph/0502313
 van Kerkwijk, M.H., van Paradijs, J., & Zuiderwijk, E.J. 1995, A&A, 303, 497
 van Paradijs, J. & Kuiper, L. 1984, A&A, 138, 71
 Webster, B.L., Martin, W.L., Feast, M.W. & Andrews, P.J. 1972, Nature Phys. Sci., 240, 183
 Wojdowski, P., Clark, G.W., Levine, A.M., Woo, J.W. & Zhang, S.N. 1998, ApJ, 502, 253
 Vrtilik, S.D., Raymond, J.C., Boroson, B., Kallman, T., Quaintrell, H. & McCray, R. 2001, ApJ, 563, L139

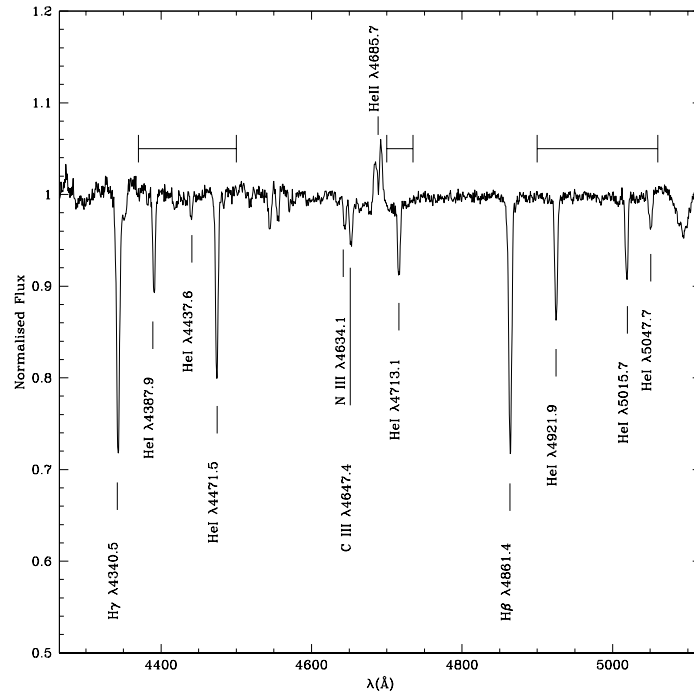


Fig. 1. The median, continuum normalised spectrum of Sk 160. The horizontal bars indicate the regions of the spectrum containing He I absorption lines used for cross-correlation and determination of radial velocities.

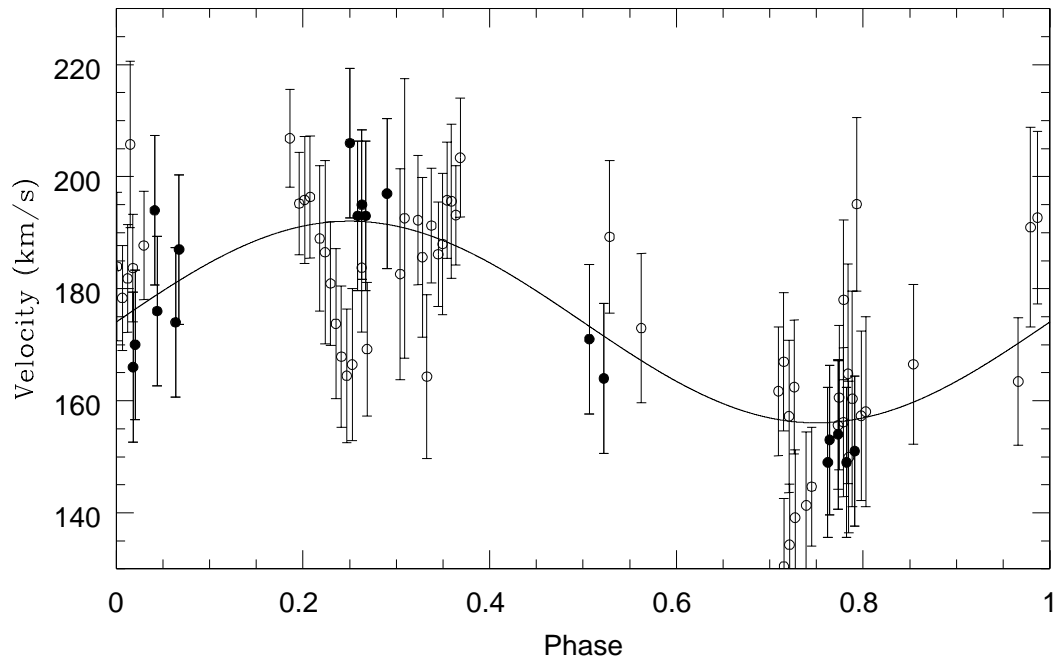


Fig. 2. The uncorrected He I absorption line RV curve for Sk 160. Our data are shown as open circles and those of Reynolds et al. (1993) are shown as filled circles. The best fit to the combined data set is indicated by the solid line.

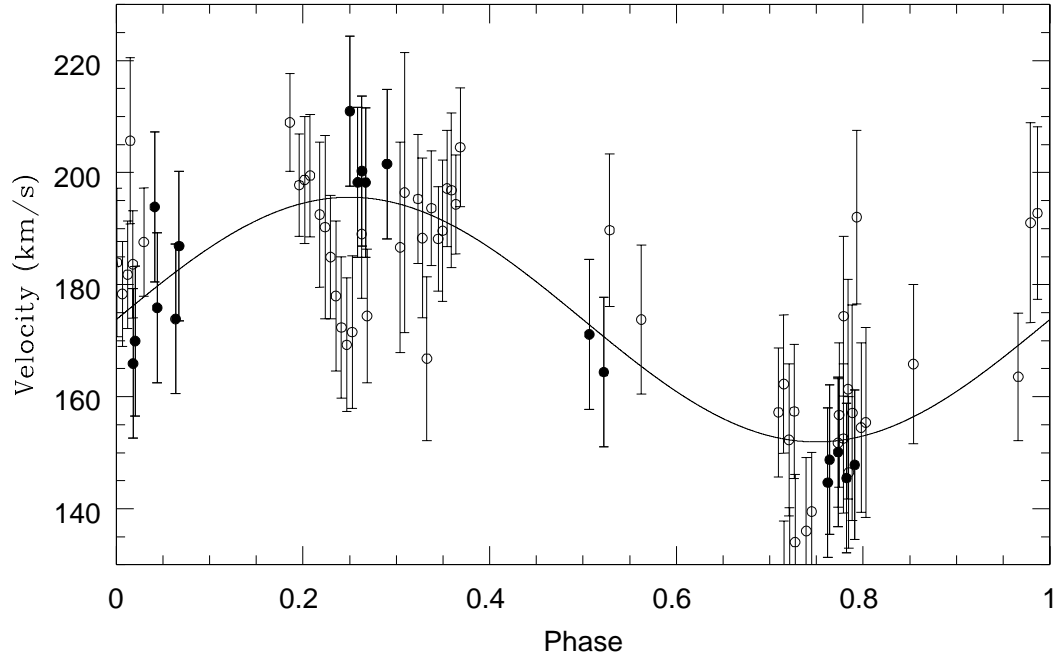


Fig. 3. The heating-corrected He I absorption line RV curve of Sk 160. Our data are shown as open circles and those of Reynolds et al. (1993) are shown as filled circles. The best fit to the combined data set is indicated by the solid line.

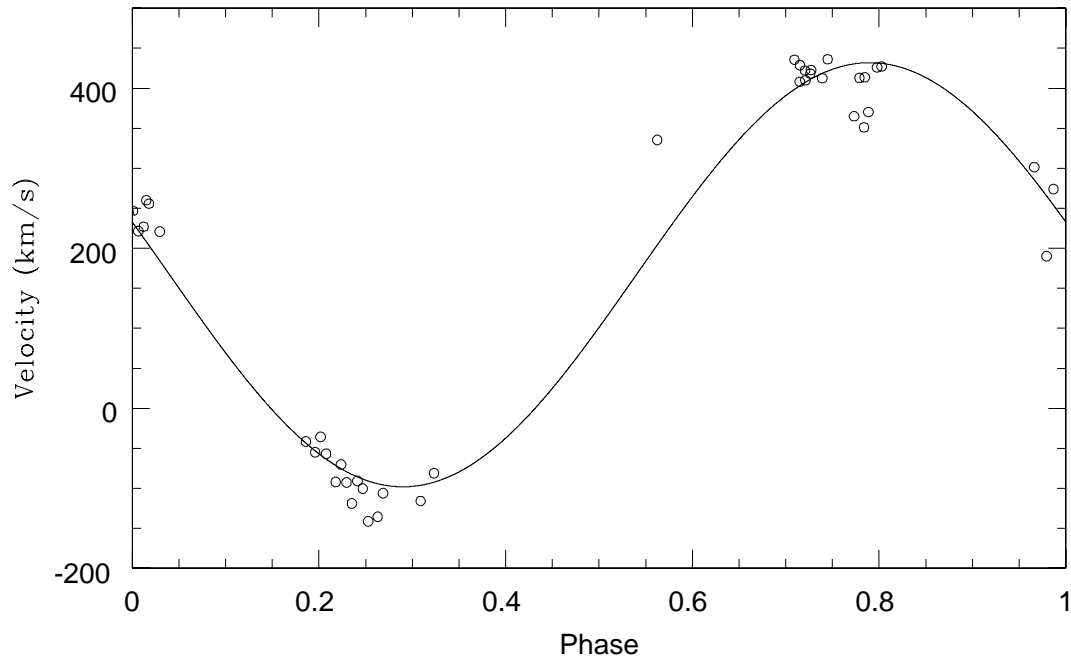


Fig. 4. The RV curve of the He II 4686Å emission line. The solid line indicates a sinusoid with a systemic velocity of 167 km s^{-1} , an amplitude of 256 km s^{-1} and a phase shift of 0.46 with respect to the Wojdowski et al. (1998) ephemeris.

Table 2. The raw and heating-corrected He I absorption line heliocentric radial velocity data for Sk 160 resulting from the August/September 2000 observations at SAAO. Also shown are the heliocentric radial velocities measured from the He II 4686Å emission line.

MJD	Phase	He I V_{raw} / km s ⁻¹	1σ uncertainty / km s ⁻¹	He I $V_{\text{corrected}}$ / km s ⁻¹	He II V / km s ⁻¹
51786.976	0.715	130	12	126	429
51786.999	0.721	134	11	129	410
51787.022	0.727	139	12	134	423
51787.069	0.739	141	13	136	413
51787.091	0.745	145	11	139	436
51788.808	0.186	207	9	209	-41
51788.847	0.196	195	9	198	-55
51788.870	0.202	196	11	199	-36
51788.892	0.208	196	11	199	-57
51788.932	0.218	189	13	193	-92
51788.955	0.224	187	16	190	-70
51788.977	0.230	181	11	185	-93
51789.000	0.235	174	13	178	-119
51789.022	0.241	168	13	172	-91
51789.045	0.247	164	12	169	-100
51789.068	0.253	166	14	172	-141
51789.108	0.263	184	12	189	-136
51789.130	0.269	169	12	174	-106
51790.845	0.709	162	12	157	436
51790.867	0.715	167	12	162	408
51790.889	0.721	157	14	152	422
51790.911	0.726	162	12	157	418
51791.094	0.773	156	11	152	365
51791.116	0.779	156	13	153	413
51791.138	0.785	150	14	146	414
51791.845	0.966	163	11	164	301
51791.896	0.979	191	18	191	190
51791.925	0.987	193	15	193	274
51791.979	0.001	184	13	184	247
51792.002	0.007	178	9	178	222
51792.024	0.012	182	10	182	227
51792.046	0.018	184	10	184	256
51792.091	0.030	188	10	188	221
51799.819	0.015	206	15	206	260
51801.817	0.528	189	14	190	
51802.774	0.774	161	13	157	
51802.792	0.779	178	14	174	
51802.811	0.784	165	20	161	351
51802.829	0.789	160	19	157	370
51802.847	0.793	195	16	192	
51802.865	0.798	157	15	154	426
51802.884	0.803	158	17	155	427
51803.083	0.854	167	14	166	
51804.836	0.304	183	19	187	
51804.854	0.309	193	25	196	-116
51804.910	0.323	192	12	195	-81
51804.928	0.328	186	14	188	
51804.947	0.333	164	15	167	
51804.966	0.338	191	10	194	
51804.994	0.345	176	9	188	
51805.013	0.350	188	13	190	
51805.031	0.354	196	10	197	
51805.049	0.359	196	14	197	
51805.068	0.364	193	9	194	
51805.086	0.369	203	11	205	
51805.841	0.562	173	13	174	335